UNIVERSITY OF CALIFORNIA,
IRVINE

Ionic Conductance of Solid Electrolytes at the Meso- and Nanoconfinement

THESIS

submitted in partial satisfaction of the requirements
for the degree of

MASTER OF SCIENCE

in Physics

by

Joseph Alex Martinez

Thesis Committee:
Professor Zuzanna Siwy, Chair
Professor Reginald Penner
Professor Phil Collins

2018

DEDICATION

To my parents,

Victor and Jennifer Martinez

TABLE OF CONTENTS

LIST OF FIGURES

ACKNOWLEDGMENTS

First, I would like to acknowledge Dr. Zuzanna Siwy; this work would not have been made possible without her support and guidance. Her patience, motivation, and enthusiasm allowed me to succeed in my research, and I could not have asked for a better advisor. Learning from her was a great privilege, and I cannot thank her enough for the opportunity to work in her lab.

I would also like to extend my deepest gratitude to my family. I am forever indebted to my parents for giving me the opportunities and experiences that have made me who I am, their love and support are worth more than can be expressed on paper. I am also grateful for the support system provided to me by my siblings, providing me with a way to remain sane during my education.

Next, I thank my friends I have made working in Dr. Siwy's lab. Without them, I could not have succeeded in my work, and I wish each of them the best in their future endeavors.

Lastly, I thank Nanostructures for Electrical Energy Storage (NEES), an Energy Frontier Research Center funded by the US Department of Energy, Office of Science, Office of Basic Energy Sciences under Award Number DESC001160 for funding this work.

ABSTRACT OF THE THESIS

Title of Thesis

By

Joseph Alex Martinez

Master of Science in Physics

University of California, Irvine, 2018

Professor Zuzanna Siwy, Chair

This thesis describes a novel approach for probing ionic conductivity of silica ionogel electrolytes on the meso- and nanoscale. These properties are important to know for the development of solid-state energy-storage devices that implement nanostructures. Silica ionogels are of specific interest because they maintain a fluidic state on the nanoscale, allowing for a high conductivity of liquid electrolytes, but on the macroscale, they maintain the stability benefits of solid electrolytes. Using single mesopores in polymer films to restrict the geometry of the ionogel to the desired size, we were able to measure the conductivity using two methods. The first method uses liquid electrolytes and makes measurements similar to how the conductivity in liquid electrolytes is found, the other method probes the solid electrolyte in a way more representative to that of energy storage devices. We concluded that the electrochemical properties of ionogel are not significantly affected by constriction to the mesoscale, meaning they can be useful in the implementation of mesoscale solid-state energy-storage devices.

INTRODUCTION

Ionic transport at the nanoscale has been at the center of interest of researchers across many different fields, and an observation of ions through nanoscale structures reveals properties not observed on the microscale[1]. Examples of these properties are cation/anion selectivity[2], rectification of ionic current[3]–[7], and sensitivity to the presence of individual molecules[8]–[11].

Due to the application of nanopores for building biological sensors and studying of biological channels the majority of research is focused onto aqueous solutions, and studies of ionic transport of non-aqueous solutions at the nanoscale remain underexplored. These types of studies can lead to important improvements in various applications, such as separations and energy storage[12], [13].

In energy storage there has also been a lot of interest surrounding the use of gel-based[14]–[16] and solid-state electrolytes[17] as a replacement of the more unstable liquid electrolytes. Our lab has performed studies of the ion current of PMMA gel containing $LiClO_4$ in propylene carbonate when constricted to a single meso-pore[18], [19]. These studies showed that this system is dependent on the pore shape, and that the gel structures rectify in current when confined to a nanopore with conical geometry. This forms the basis for a solid-state ionic diode. This type of system has also been shown to be very stable.

Our work seeks to examine the ion transport properties of silica ionogel[20] that has been deposited into polymer pores on the meso- and nanoscale. Ionogels are basically ionic liquid, trapped in a rigid nanoporous structure, and these generally have larger

conductivity than other electrolytes due to the fact they maintain a fluidic conductance on the nanoscale. Because of this they make a great alternative to other solid-state electrolytes.

CHAPTER 1: THEORY

Ion transport in meso- and nanopores has gained significant attention in recent years not only due to the growing need for better performing battery systems but also in search of new physical phenomena that govern ionic distributions and transport under confinement. Single nano- and mesopores with well-defined geometry and chemical properties become an ideal testbed for probing these transport properties. It is because transport properties of one pore can be directly correlated with the pore's electrochemical properties.

Ionic transport at the confinement is a combination of behaviors of fluid transport via diffusion and electrokinetics, with phenomena that occur due to the large surface to volume ratio, such as the electrical double layer with a size that is relevant to the size of the system.

1.1: ION TRANSPORT

Mathematically, ionic transport in nanopores can be described using the continuum approach applicable also to macroscale. We will start with derivation of the Nernst-Plank equation, which describes ionic flux due to concentration gradient (diffusion) and electrical potential gradient. Equation (1.1) demonstrates Fick's law of diffusion in 1 dimension[21].

$$j_{aff} = -D\frac{dC\ (x)}{dx} \tag{1.1}$$

where, j_{diff}, is a flux of ions that is proportional to the concentration gradient of species, with diffusion coefficient, D, being the proportionality constant. If concentration of species is a function of both space and time, there is a continuity equation form of:

$$\frac{dC(x,t)}{dt} = -\frac{dj(x,t)}{dx} \tag{1.2}$$

Plugging Fick's first law into this we can find that the time evolution of a system $C(x,t)$:

$$\frac{dC\ (x,t)}{dt} = D\frac{d^2C\ (x,t)}{dx^2} \tag{1.3}$$

When electric field is applied in the system, electromigration of ions needs to be considered as well. We will start by defining the velocity at which these ions move in a solution as:

$$v_{drift}(x,t) = \frac{qE(x,t)}{\zeta} \tag{1.4}$$

In this equation V_{drift} is the drift velocity of the ion, q is the charge of the ion, E is the electric field applied to the system, and ζ is the drag coefficient of the ion. We know that flux is the product of the concentration of ions multiplied by the velocity at which they are traveling:

$$j_e(x,t) = v_{drift}(x,t)C(x,t) \quad 1.5$$

Replacing the drift velocity in equation (1.5) with what our definition of drift velocity of an ion, equation (1.4), we can find an expression for the electrophoretic flux, equation (1.6).

$$j_e(x,t) = \frac{qE(x,t)}{\zeta}C(x,t) \quad 1.6$$

This equation provides description of how an electric field effects the movement of species. We can express drag coefficient, ζ, in terms of diffusion coefficient, D, using the Einstein-Smoluchowski's equation:

$$\zeta = \frac{k_B T}{D} \quad 1.7$$

By plugging equation (1.7) into equation (1.6), we find that the 1-dimensional electrophoretic flux becomes:

$$j_e(z,t) = D\frac{qE(x,t)}{k_B T}C(x,t) \quad 1.8$$

Adding the electrophoretic flux, equation (1.8), to Fick's law, equation (1.1), and generalizing to three dimensions, we can describe the total flux of a single species of ion as follows:

$$j\,(z,t) = -D(\nabla C + \frac{qC}{k_b T}\nabla\phi) \quad 1.9$$

This can be generalized further to the following, which is the flux of all ions present in a solution:

$$j_{tot}\,(z,t) = \sum_{i} -D_i(\nabla C_i + \frac{q_i C_i}{k_b T}\nabla\phi) \qquad 1.10$$

The index *i* is used to denote a single ion type with diffusion coefficient D_i, concentration C_i, and charge z_i.

1.2: DEBYE LAYER

So far in our discussion of ion transport we have only considered the behaviors that are also relevant to macroscopic transport. Since, the ultimate goal of the project is to identify the properties of an electrolyte confined in a nanopore, we need to consider the effects of the surface of the pore on local ionic concentrations and transport.

In the experiments described in future chapters, we use pores that have a negative surface charge on the walls. Due to the presence of this charge, there are electrostatic interactions between the pore surface and the ions in the solution that create formation of

an electrical double layer. Consequently, there is a region close to the pore walls with enhanced concentration of counterions. This can be seen in the figure 1.1.

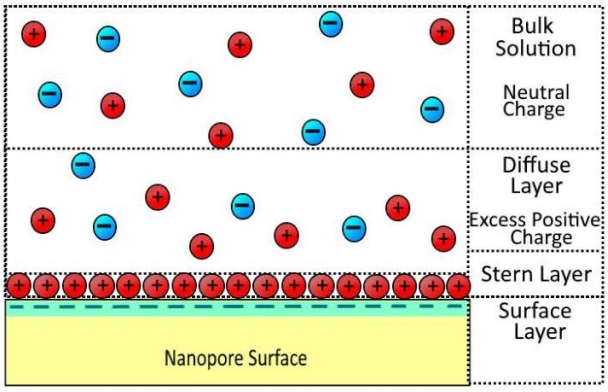

Figure 1.1 The Electric Double-Layer at a charged interface.

Due to the large surface area to volume ratio of our system, we could simply model the pore wall as an infinite plane and find the solution of how charges interact with this system.

The system will be described starting from the Poisson equation, expressed as a function of the concentration of particles.

$$\nabla^2\phi(x) = -\sum_i \frac{Fz}{\varepsilon} C_i(x) \qquad 1.11$$

We will consider the Boltzmann distribution describing the concentration of an ion at a distance, x, from the wall, characterized with electric potential, $\phi\ (x)$:

$$C(x) = C_0 e^{\frac{-ez\phi(x)}{k_B T}} \qquad 1.12$$

In our experiments we typically use so-called 1:1 electrolyte with monovalent cation and monovalent anion (e.g. KCl or $LiClO_4$), so that the net charge in the solution is equal:

$$\rho(x,t) = zeN_A C_0 (e^{\frac{-ez\phi(x)}{k_B T}} - e^{\frac{ez\phi(x)}{k_B T}}) \quad 1.13$$

This equation can be simplified into the trigonometric form:

$$-2zeN_A C_0 \sinh\left(\frac{ez\phi(x)}{k_B T}\right) \quad 1.14$$

Which for small surface potentials (significantly lower than $k_B T$) can be simplified using the small angle approximation as:

$$\rho(x) = \left[\frac{2e^2 z^2}{\varepsilon k_B T}\right]\phi(x) \quad 1.15$$

The leading term has units of $\frac{1}{m^2}$, and we call this distance the Debye length, λ_D. This gives us the final version of our equation:

$$\rho(x) = \frac{\phi(x)}{\lambda_D^2} \quad 1.16$$

$$\lambda_D = \sqrt{\frac{\varepsilon k_B T}{2e^2 z^2 C_0}} \quad 1.17$$

Using the boundary conditions that $\phi = \phi_{surface}$ at $x = 0$, and $\phi = 0$ at $x = \infty$, we find an equation for the potential at a given distance z from the pore wall[22].

$$\phi(x) = \phi_{surf} e^{-\frac{x}{\lambda_D}} \quad 1.18$$

1.3: IONIC LIQUID TRANSPORT PROPERTIES

In solutions with a very high concentration of ions, the ions become positioned close enough that one needs to consider the interactions between nearest neighbor ions[23], which can involve energies on the order of $5 - 10\ k_B T$. This means that the Debye length approximation above should no longer hold true. In aqueous solutions however, due to the high dielectric constant of water, even when the ions get closer than the Bjerrum length, the interionic interactions become much smaller than the thermal energy. Because ionic liquids do not contain water, it is unclear if we need to consider the short-range interactions. To understand this, we will consider the mean-field lattice-gas model of concentrated electrolytes. We start with the free energy of the system, which is seen in equation (1.19)

$$F = \frac{e}{k_B T}\phi(z_+ N_+ - z_- N_-) + B_+ N_+^2 + B_- N_-^2 + C N_+ N_- - k_B T\ ln(W) \quad 1.19$$

Here z_+ and z_- are the valencies of the cations and anions respectively, in general they are opposite and equal in value. N_+ and N_- are the number of cations and anions, and ϕ is the electrostatic potential. B_+ is a constant that characterizes the non-Coulomb

interactions between cations, B_- is a constant that characterizes the non-Coulomb interaction between anions, and C represents the non-Coulomb interactions between a cation and an anion. The final term describes the entropy that stems from the distribution of ions over available sites. Given that there are N total sites available for the ions to occupy, we can find that the number of combinations for the cations to occupy is:

$$W_+ = \frac{(N - N_-)!}{(N - N_+ - N_-)!\, N_+!} \tag{1.20}$$

We can similarly find that the number of combinations for the distribution of anions is:

$$W_- = \frac{(N - N_+)!}{(N - N_+ - N_-)!\, N_-!} \tag{1.21}$$

And finally, we consider the distribution of holes that are unoccupied by a cation or anion:

$$W_h = \frac{N!\ (N - N_-)!}{(N - N_+ - N_-)!\, (N - N_+)!\, (N - N_-)!} \tag{1.22}$$

Multiplying these three terms together to find W,

$$W = \frac{N!}{(N - N_+ - N_-)!\, N_+!\, N_-!} \tag{1.23}$$

Giving us the equation for free energy as:

$$F = e\phi(z_+N_+ - z_-N_-) + B_+N_+^2 + B_-N_-^2 + CN_+N_- - k_BT\ln\left(\frac{N!}{(N-N_+-N_-)!N_+!N_-!}\right) \quad 1.24$$

We will apply Stirling's approximation to the logarithm and take the derivative to find the electrochemical potential expressions for the cations and anions. We will also take $z_+ = -z_- = 1$ and find the following equations:

$$\mu_+ = \frac{\partial F}{\partial N_+} = e\phi + 2B_+N_+ + CN_- - k_BT\ln\left(\frac{N_+}{N - N_+ - N_-}\right) \quad 1.25$$

$$\mu_- = \frac{\partial F}{\partial N_-} = e\phi + 2B_-N_- + CN_+ - k_BT\ln\left(\frac{N_-}{N - N_+ - N_-}\right) \quad 1.26$$

At this point we can make the assumption that the non-Coulomb interactions are much smaller than the other interactions, meaning that $B_+ \approx B_- \approx C \approx 0$. Therefore, our expressions for electrochemical potentials become:

$$\mu_+ = e\phi - k_BT\ln\left(\frac{N_+}{N - N_+ - N_-}\right) \quad 1.27$$

$$\mu_- = e\phi - k_BT\ln\left(\frac{N_-}{N - N_+ - N_-}\right) \quad 1.28$$

By assuming the system is in equilibrium, we can set the electrochemical potential in equations 1.27 and 1.28 equal to the electrochemical potential in the bulk we can rewrite these two equations we can find the concentration of the individual ions as follows:

$$c_+ = \frac{c_0 \exp\left(-\frac{e\phi}{k_B T}\right)}{1 - \gamma + \gamma \cosh\left(\frac{e\phi}{k_B T}\right)} \tag{1.29}$$

$$c_- = \frac{c_0 \, exp\left(\frac{e\phi}{k_B T}\right)}{1 - \gamma + \gamma \, cosh\left(\frac{e\phi}{k_B T}\right)} \tag{1.30}$$

where $\gamma = (N_+ + N_-)/\, N \; = 2c_0/c_{max}$. We can then find the charge density by simply adding the charges from the individual concentration of ions, as seen in equation (1.31).

$$\rho = e(C_+ - C_-) = -2ec_0 \frac{Sinh\left(\frac{e\phi}{k_B T}\right)}{1 + 2\gamma \, sinh^2\left(\frac{e\phi}{2k_B T}\right)} \tag{1.31}$$

In the case that the concentration of ions is low, the interactions between ions can be ignored, so that $\gamma = 0$; combining eq. (1.31) with the Poisson equation, the Poisson-Boltzmann equation is obtained[23]. With finite γ, we obtain (1.32).

$$\frac{d^2\Phi}{dx^2} = -\frac{4\pi\rho}{\epsilon} = \frac{8\pi e c_0}{\epsilon} \frac{Sinh\left(\frac{e\phi}{k_B T}\right)}{1 + 2\gamma \, sinh^2\left(\frac{e\phi}{2k_B T}\right)} \tag{1.32}$$

We will now change to dimensionless variables to simplify our expression. We will use a dimensionless potential defined by:

$$u = \frac{e\phi}{k_B T} \tag{1.33}$$

and we will modify our distance by the Debye length:

$$X = \frac{x}{\lambda_D} \tag{1.34}$$

Plugging the unitless variables into equation (1.32), we find the Poisson's equation becomes:

$$\frac{d^2\mathrm{u}}{dX^2} = \frac{sinh(u)}{1 + 2\gamma \sinh^2\left(\frac{u}{2}\right)} \tag{1.35}$$

We will use the same boundary conditions as before, i.e. the potential is u_0 at the boundary of the electrode or charged surface $X = 0$, and 0 when $X \gg 1$. Equation (1.35) cannot be solved for an explicit expression $u(X)$, so instead we solve for the inverse function $X(u)$. We find that equation to be:

$$X = sgn(u_0)\sqrt{\frac{\gamma}{2}}\int_u^{u_0} \frac{du}{\sqrt{ln\left(1 + 2\gamma \sinh^2\left(\frac{u}{2}\right)\right)}} \tag{1.36}$$

This can be calculated using numerical methods for any given value of u, u_0, and γ. From this one can numerically find the potential $u(X)$. In the case that γ tends to zero we can find the solution to be:

$$\mathrm{u(X)} = 2\ln\left(\frac{1+\tanh\left(\frac{u_0}{4}\right)\exp(-X)}{1-\tanh\left(\frac{u_0}{4}\right)\exp(-X)}\right) \qquad 1.37$$

Equation (1.37) is well-known in the Gouy-Chapman theory, however in the case of ionic liquids, it cannot be applied. With γ closer to 1, due to the large number of ions present, there are solutions where lattice saturation occurs, meaning that the ions cannot pack densely enough close to the surface to screen very high surface charges in just one layer of ions, instead it takes several layers. The number of layers required to screen the surface potential, and thus the thickness of the double layer, grows with the applied potential, which is not the case in classical solutions as described by equation (1.17).

The behavior of ionic liquids near charges has been modeled[24] and can be seen below in figure 1.2. Ionic distributions close to the surface demonstrate that there are oscillations in the charges seen in the double layer and are not simply exponential as is the case with other liquid electrolytes. Figure 1.2 shows the effect of overcharging e.g. the negatively charged surface is first over-screened by counterions, so that the net positively charged layer is now screened with anions, etc.

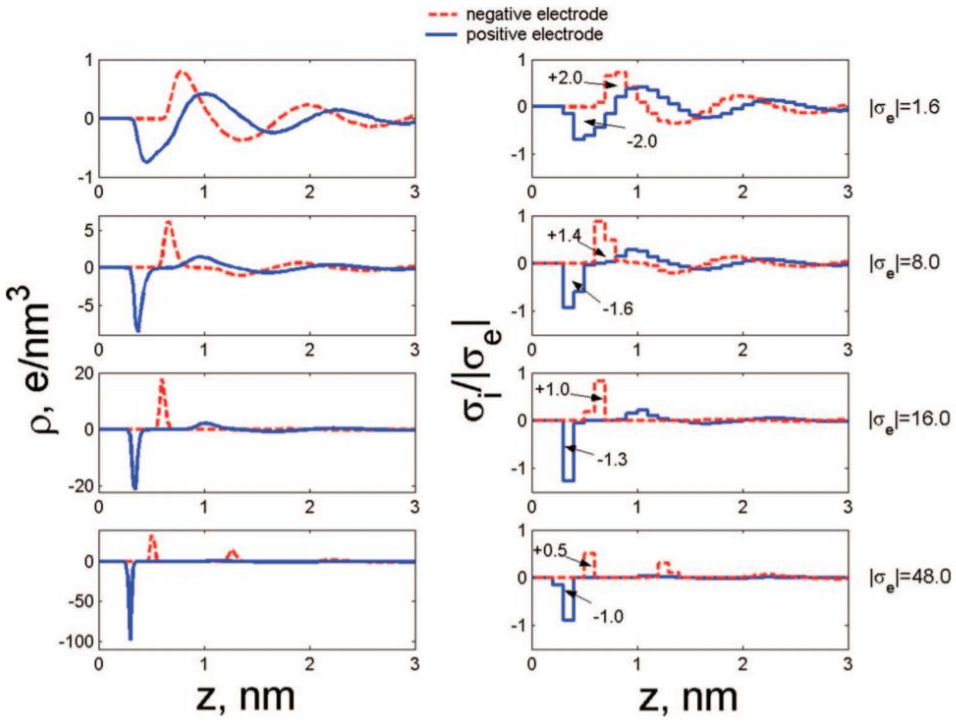

Figure 1.2 Modeled electrical double layer of the ionic liquid near the anode (solid/blue lines) and cathode (dashed/red lines). Reprinted with permission from ref. [24] Copyright 2008 American Chemical Society.

CHAPTER 2: SAMPLE PREPERATION

Single meso- and nanopores were prepared in 12 micrometers thick polyethylene terephthatalate (PET) films by the track-etching technique. Track-etching consists of two steps, heavy ion radiation, and wet chemical etching, which determines the pore size and shape. The number of pores is determined by the number of heavy ions used in irradiation: each heavy ion leads to preparation of one pore. In the experiments we used silica ionogel, which was synthesized by Dr. Bruce Dunn's group at the University of California, Los Angeles by use of a low temperature sol-gel synthesis procedure. Single pores in polymer films were filled with the ionogel by the process of drop casting on both sides of the membrane. Ion transport properties of the confined ionogel were measured and used to quantify ionic conductivity of the ionogel as a function of the pore diameter.

2.1: FABRICATION OF POLYMER MESO- AND NANOPORES

The 12 micrometer thick films of polyethylene terephthatalate (PET) used in our experiments were first irradiated with single energetic heavy ions (gold or uranium) at the UNILAC linear accelerator at the GSI accelerator center in Darmstadt, Germany. At GSI, for single-ion irradiation, ions with energy of 11.4 MeV (equivalent to ~2GeV of total kinetic energy) are used. This energy allows for the penetration of up to about 100 micrometers of PET [25], therefore multiple membranes, usually 6 stacked together, are irradiated at the same time. These membranes are then shipped to our lab for chemical etching.

Membranes are then exposed to UV radiation from a desktop UV lamp (UVP 95-0021-12) at a wavelength of 365nm for 45 minutes to 1 hour per side. Due to the effect of UV radiation on polymer structures[26], [27] this step increases the etch rate of the damaged tracks by up to three or four times. It is believed that the irradiation causes breaks in the polymer chains by exciting the electrons in the polymer. The energy from the excited electrons is then changed into thermal fluctuations, moving the atoms from their preferred position. These sites where the chain is broken is more reactive to the etchant solution.

After irradiation, the polymer film is then subjected to wet chemical etching. The type and concentration of the etchant as well as conditions of etching (temperature, time and configuration) determine the pore geometry and pore opening. [28] Irradiated PET films are etched using sodium hydroxide (NaOH) which attacks the PET monomer at the ester bond in a depolymerization mechanism known as alkaline hydrolysis [29]. This process leaves carboxyl groups exposed on the etched surface, giving the pore a negative surface charge in a neutral pH.

In order to prepare a cylindrically shaped PET, an irradiated PET film is etched in 2M NaOH held in a heat bath at 60 °C . A PET pore is submerged in the heated NaOH solution and will remain submerged for a period of time that will roughly etch a pore with a desired diameter. We have found that under these conditions, the PET will etch at a rate around 1 micrometer in diameter per hour of etching.

After rinsing the now etched pore in distilled water, the diameter is measured by applying a transmembrane potential across the pore filled with a solution of known conductivity. This would result in a linear IV curve such as that seen in Figure 2.1, where

the slope of the curve, by ohm's law, is the resistance of the pore. We can now treat the pore like a resistor and solve for its geometry[27].

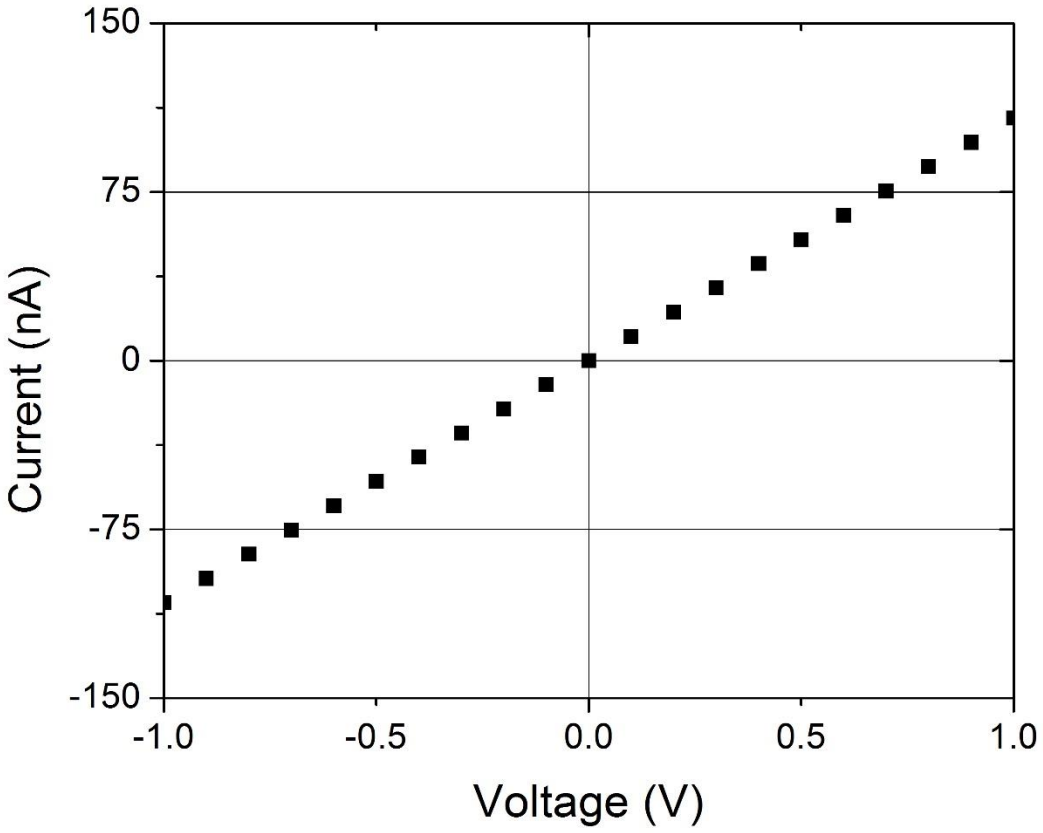

Figure 2.1: Example of current-voltage curve for 400nm pore in 1M KCl

Using the formula that relates the resistance of the pore, to the conductivity of the electrolyte we can find the diameter. The formula is as follows:

$$R = \frac{4L}{\sigma * \pi * D^2} \tag{18}$$

Where σ is the resistivity of the electrolyte, L is the thickness of the membrane, and D is the diameter of the pore, seen in the Figure 2.2 below.

The pore diameter is typically measured using 1 M KCl as the background electrolyte. The high concentration solution assures screening of the pore walls surface charges so that one can assume that the conductivity of the medium in the pore is equal to the conductivity of the bulk solution. Moreover, mobility of potassium and chloride is nearly identical, thus there is no potential difference developed due to differences in ions mobility.

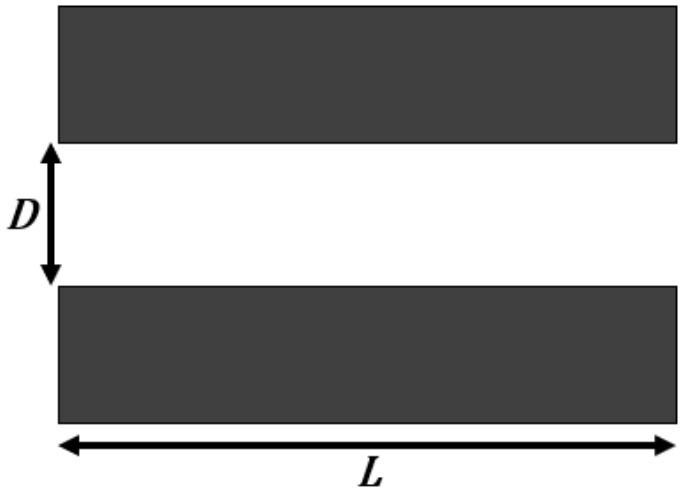

Figure 2.2: Schematic of the geometric definitions of a cylindrical pore, see eq. 18.

To test the properties of ionogel at the nanoscale we used conical pores that had a tip diameter measuring between 20 nm and 100 nm. To prepare these pores we used a single-sided etching technique[30] that has the membrane held in a conductivity chamber with one side of the chamber containing an etchant solution and the other chamber containing a neutralizing solution.

Conical pores are obtained when the etchant: 9M NaOH is placed on the side of the membrane, and the other side is contact with a neutralizing solution of 1M formic acid in 1M KCl. The side of the membrane exposed to NaOH will contain the large opening of a conical pores, called the base; the side of the membrane in contact with the neutralizing agent with have the narrow opening, called tip. The etching is performed while monitoring the current at 1 V. The voltage is applied in such a way that the hydroxide ions, which participate in the process of etching, are electrophoretically pulled from the narrow opening, which helps to control the pore opening diameter. The etching is stopped when current of ~1 nA is observed, at which point the solutions are removed and we define the geometry in a similar method as the cylindrical pores.

Current-voltage curves of conical nanopores with the tip opening of ~60 nm and smaller are often rectifying at higher voltages, so that currents for voltages of one polarity are higher than currents for the opposite polarity, as seen in figure 2.3. The property of rectification makes it unclear on how the resistance would be measured. In order to get an estimation of the resistance of the pore, and the pore opening diameter, current-voltage curves are taken at low voltages (below 0.5 V), where the pore is Ohmic, figure 2.4.

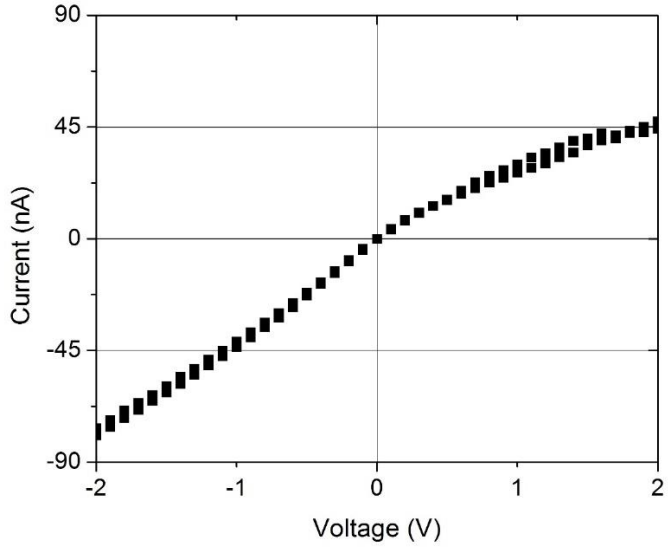

Figure 2.3: An example current-voltage curve of a single conical nanopore recorded in 1M KCl. This pore had opening diameter of 60 nm, as calculated from the linear part of the I-V.

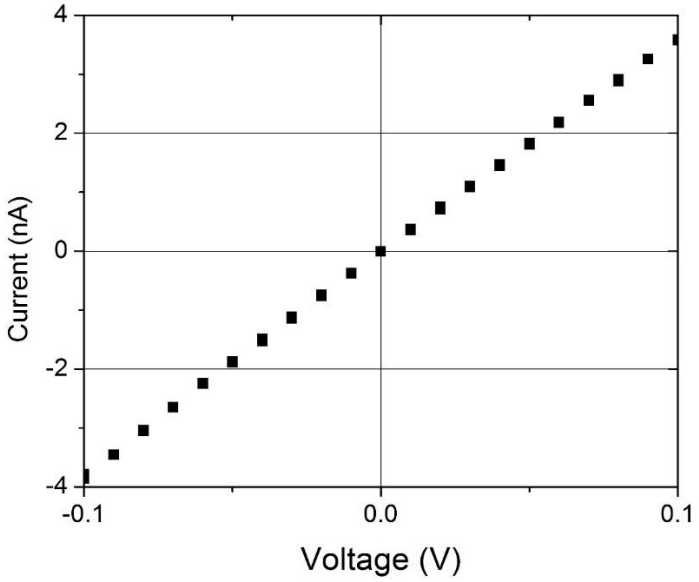

Figure 2.4: Linear region of figure 2.3 current voltage curve in linear region of conical pore in 1M KCl.

From this we use Ohm's law, once again, to find an estimation for the resistance of the pore. We can then use a similar method to find the geometry of the pore. The equation that relates the geometry of the pore to the conductivity of the electrolyte and the resistance of the pore is seen below.

$$R = \frac{4L}{\sigma * \pi * d * D} \tag{19}$$

Parameters d and D indicate the tip and the base diameter, respectively, Figure 2.5. The base diameter, D, is found by taking the known bulk etch rate of PET in 9M NaOH[30] and multiplying it by the etching time and a factor of 2 due to isotropic character of the bulk etching.

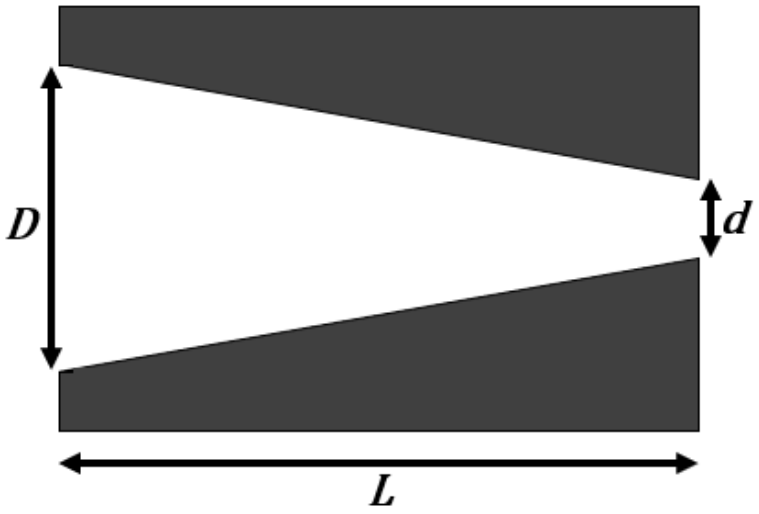

Figure 2.5: Schematic of the geometric definitions of a conical pore

2.2: SYNTHESIS OF IONOGEL

The ionogel used in these experiments was synthesized by David Ashby and Dr. Bruce Dunn using a low temperature sol-gel synthesis procedure.[20] This process used the hydrolysis of Tetramethylorthosilicate, (TMOS), triethylvinylorthosilicate, (VETOS).

In this process equal volumetric amounts of TMOS, VETOS, and formic acid were sonicated until mixed. This differs from other processes through the use of VETOS which results in improved structural stability of the ionogel[31]. This is the silicate precursor solution that will create the silicate structure of the ionogel.

A 3/3/1 volumetric ratio of the silica precursor solution/ Ionic liquid electrolyte/cyclohexane was prepared and aged for 4 hours at -20 °C before processing (1.4/1/5.6/2.1/2.1 mole ratio). This resulted in an ionogel sol, which had a low enough viscosity to penetrate the entire pore. The ionogel sol is allowed to dry in ambient conditions, causing a continuous mesoporous silicate matrix to form. Due to the very low vapor pressure of the ionic liquid, it does not evaporate during the sol-gel process. This results in the silicate matrix filled with the ionic liquid trapped in the structure by capillary forces.

The ionogel's silicate structure can be seen in figure 2.6, which shows voids in the structure to be about 10nm in diameter. Studies show that roughly 80% of the ionogel's volume is made up of the ionic liquid present in the ionogel supporting the claim that the voids are highly interconnected. It was also demonstrated that ionic liquid containing a lithium salt undergoes destructuring when confined in silica structure of the ionogels.[34] The effect of destructuring causes ion pairs to become destabilized, which results in an increased conductivity.

Figure 2.6. TEM imaging of the structure of ionogel with ionic liquid removed through super critical drying.

2.3: ELECHTROCHEMICAL CHARACTERIZATION OF IONOGELS

Two methods were used to measure the ion transport properties of the ionogel, and they differ in the electrodes configuration, and the type of bulk electrolyte. In the first method that will be described, ~20μL of ionogel sol is drop casted directly onto the PET membrane to fill the entire pore with the electrolyte. The film is then placed between two chambers of the conductivity cells filled with ionic liquid BMIM TFSI containing 500 mM Li TFSI; this is the same electrolyte as present in the ionogel. Pellet Ag/AgCl electrodes (A-M Systems, Sequim, WA) were used in the measurements. This technique is similar to the process used to measure the properties of a liquid electrolyte[1], and can be seen in the schematic in Figure 2.7.

Figure 2.7: Single pore filled with ionogel placed in contact with an ionic liquid with lithium salt; two electrodes are place in the liquid. The PET membrane is shown in grey, ionic liquid in blue, and the patterned region represents the casted ionogel. The arrows show the two electrodes labeled “W” for working and “G” for ground.

The second method used to probe the properties of ionogel was done without the use of the bulk ionic liquid. The PET membrane has 20 nm thick gold stripes sputtered onto each side. These gold stripes are then used as the electrodes for the tests done on ionogel. The pores then have around 20μL of ionogel sol drop casted onto them such that they fill the pore and only partially cover the gold so that electrodes can be attached to the gold. A schematic can be seen in Figure 2.8.

Figure 2.8: Single pore filled with ionogel placed in contact with gold electrodes deposited onto the surface of the PET membrane. The PET membrane is shown in grey, gold electrodes are shown in yellow, and the patterned region represents the casted ionogel. The arrows show the two electrodes labeled “W” for working and “G” for ground.

CHAPTER 3: EXPERIMENTS

3.1: IONIC CONDUCTIVITY

One of the transport properties that we are interested in is the ionic conductivity of ionogel when constricted down to the nanoscale. With the recent work to implement nanostructures into the design of batteries, it becomes important to know how electrolytes work on this scale. To probe this property, we used meso- and nanopores with ionogel deposited in it, as described in the previous chapter.

We first probed the ionic conductivity on the mesoscale using the set up shown in figure 2.3. The PET membrane is used to separate the two chambers of a conductivity cell filled with the same ionic liquid that is present in the ionogel, BMIM TFSI containing 500 mM Li TFSI. These measurements were taken with the use of pellet Ag/AgCl electrodes to apply the transmembrane potential. These measurements of the ion current through the material is similar to the method that is used to measure liquid electrolytes. Figure 3.1 shows the results from a current-voltage curve obtained from using this method.

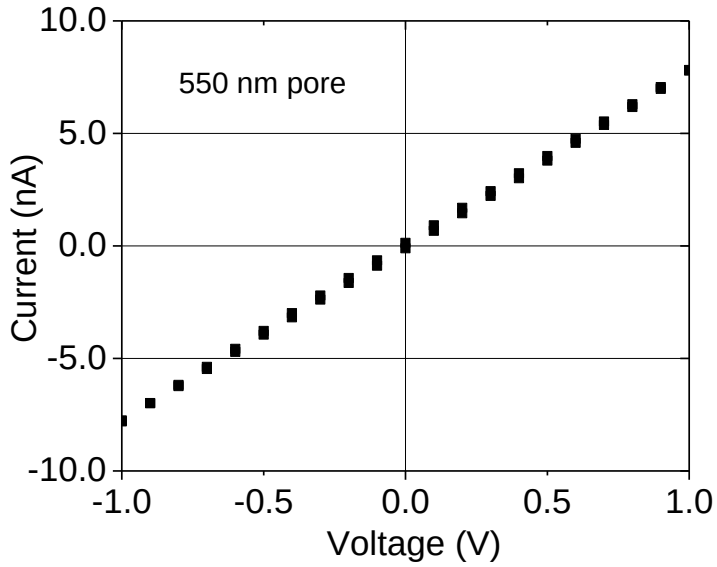

Figure 3.1: Example of a current-voltage curve recorded from a 550 nm in diameter cylindrical pore filled with ionogel.

The pore that was used in this measurement had a length of about 12 micrometers and diameter of 550 nm as measured by the methods described in the previous chapter. The current-voltage curve of this pore was linear, allowing us to calculate the resistance of the confined ionogel through Ohm's law.

$$R = \frac{V}{I} \tag{3.1}$$

Using the pore resistance and the known geometry of the pore we are able to plug back into the equation relating the resistance to the conductivity of the medium filling the pore.

$$\sigma = \frac{4L}{R\pi d^2} \qquad 3.2$$

Six additional measurements were taken from pores that were prepared independently of one another and their conductivities were plotted versus the pore diameter, the results of which can be seen in figure 3.2. This figure indicates that there is no strong dependence on the diameter of the pore, meaning that ionogel is not heavily affected by constriction to the mesoscale. The experiments gave an average ionic conductivity of the ionogel for all pores of 0.39 S/m, which is in agreement with previous data obtained in the ionogel films.[32]

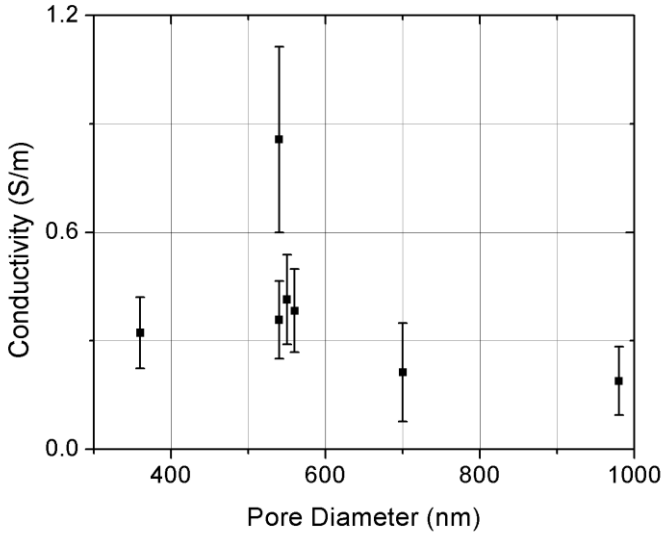

Figure 3.2: Conductivity of ionogel measured with seven independently prepared single-pore membranes.

The second method used to measure ionic conductivity of the ionogel did not involve bulk ionic liquid. This created a set up more closely related to the experiments

performed in the solid-state battery set-up. The electrical contacts were provided by the 20nm thick layer of gold that was sputtered onto the membrane after the pore was etched. The ionogel deposition is done in a way such that the ionogel covered only part of the gold on the membrane surface, so that sufficient amount of gold was left to establish electrical contact. There was still an excess of ionogel on the membrane surface, which served as the source of ions. We do not believe that any depletion zones were formed with voltage on due to the presence of only a single pore and low values of currents recorded. The ion current measured is a sum of ion currents carried by all ions present in the solution, thus not only lithium and TFSI but also ions that compose the background ionic liquid. An example current-voltage curve obtained in the liquid-electrolyte free set-up is shown in Figure 3.3 which again shows ohmic behavior.

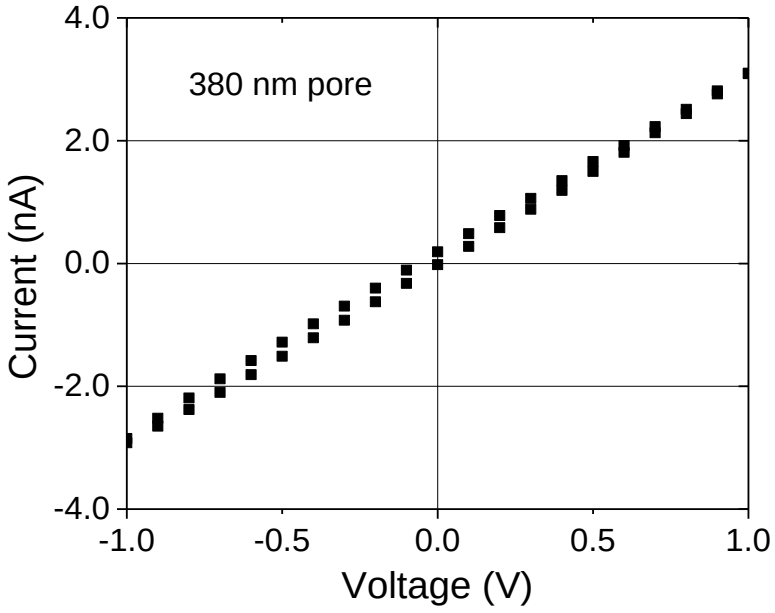

Figure 3.3: Example of a current-voltage curve recorded from a 380 nm cylindrical pore filled with ionogel without the bulk ionic liquid in the conductivity cell.

Measurements such as shown in Figure 3.3 allowed us to calculate ionic conductivity of the ionogel using the same equations as before, eq. 3.1 and 3.2. Five single-pore membranes with gold contacts and deposited ionogel were prepared; ionic conductivities of the ionogel plotted versus their pore diameters can be seen in figure 3.4. This figure indicates that the values of ionic conductivity measured are independent of the diameter of the pore, and they are similar to the values measured in the set up that involved liquid electrolyte on both sides of the membrane (Figure 3.2). Again, this leads to the conclusion that the ionogel is not heavily affected by the constriction to the mesoscale.

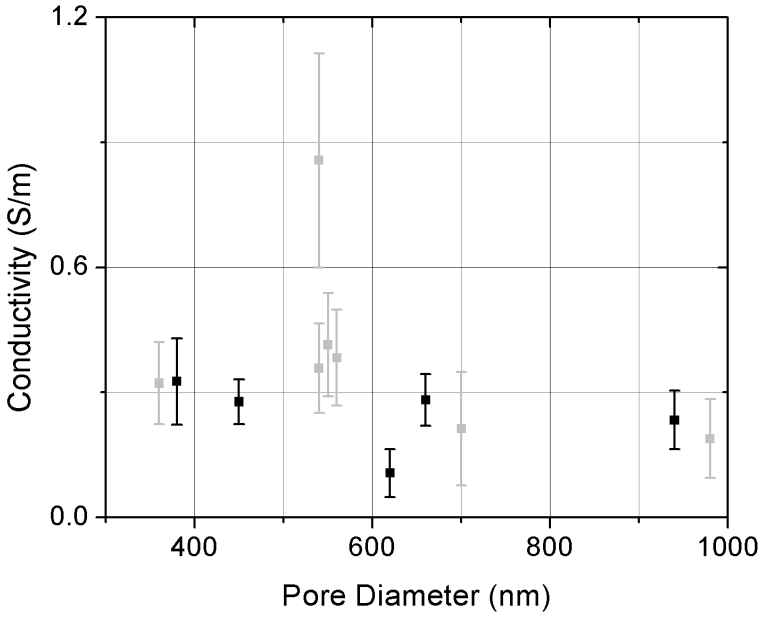

Figure 3.4: Conductivity of ionogel measured with five independent samples of single-pore membranes. The measurements were taken without bulk ionic liquid in the conductivity cell. The electrical contact was established via Au deposited prior to drop-casting ionogel. Data from Fig. 3.2 included in grey for direct comparison.

The first conclusions that we can take from the Experimental results shown in figure 3.2 and 3.4 is that the presence of the bulk liquid electrolyte does not have a significant effect on the conductivity of the ionogel. This means that the transported ions are sourced from the excess ionogel that was deposited onto the surface of the membrane, and no depletion zone is formed. The data also suggest that the resistance of the interface between the ionic liquid and the ionogel did not contribute to the resistance of the system. The final conclusion from this set of experiments is that the ionogel conductivity, which is in agreement with studies on the bulk material, is not affected by the reduction of size from the macroscale to the mesoscale.

The fact that the conductivity is independent of the diameter of the pore also suggests that the structure of ionogel is preserved inside of the pore. Previous structural studies show that the ionogel is composed of interconnected voids of about 10nm[20], [32], as seen in figure 2.6. This was also confirmed in our experiments via the finite current through a pore filled with ionogel.

As the next step, we probed ionic conductivity of the ionogel at the nanoscale. To do this we performed experiments with single nanopores that were conical in shape and had a tip diameter less than 100 nm. In order to ensure that the ionogel filled the entire volume of the pore, we used conical nanopores with the base opening as large as 1 micrometer. We performed the same type of current-voltage measurements as done for the cylindrically shaped pores. An example measurement performed in the configuration without the bulk ionic liquid present is shown in figure 3.5.

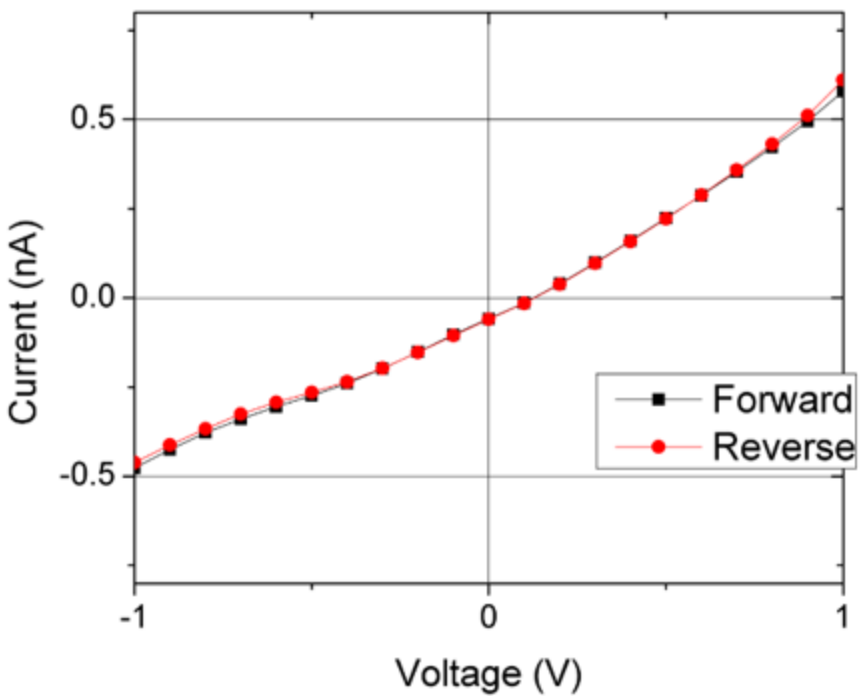

Figure 3.5: Current-voltage curve of a conically shaped nanopore filled with the ionogel. The pore opening diameter was 20 nm. The nonzero current at 0V is caused by instrument offset.

Measurements of ion current as a function of time were performed as well using sampling frequency of 10 kHz. We took 100-second-long recordings at each voltage step between -1V and +1V, the results of this test can be seen in figure 3.6. The data confirmed our previous conclusion on the excess ionogel present at the surface as sufficient source of ions –no signal decay occurred during the 100-second-long recording at each voltage. The second conclusion is that the current was stable in time, i.e. it did not fluctuate as observed before for some nanopores in aqueous environment.

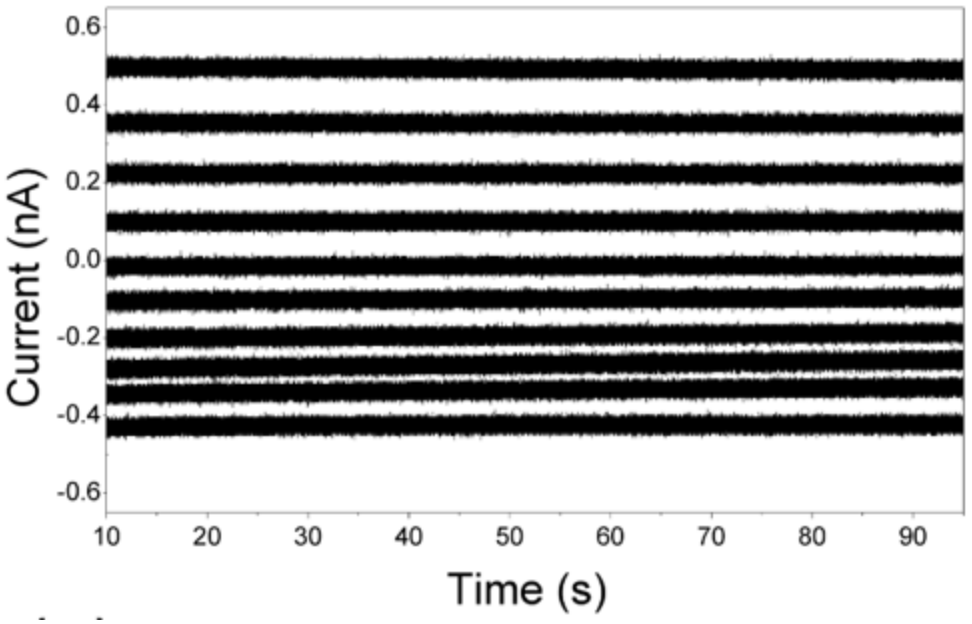

Figure 3.6: Ion current through ionogel deposited into a single conical nanopore with an opening of 20nm (tip) and 1 μm (base). Signals were recorded between -1V and +1V with a 100mV step.

3.2: SURFACE CHARGES

Another important area of study for electrolytes is their ability to screen surface charges. In nanopores with finite surface charges, it is possible to observe a selective transport of counterions to the charges on the pore walls. Silica backbone of the ionogel is negatively charged, however in contact with an ionic liquid, one could expect the charges to be largely screened due to the large number of ions present in the solution. Moreover, Li^+ ions were shown to adsorb on surfaces reducing the effective surface charges further.[1]

To probe the surface charges of the system, a method know as Scanning Ion Conductance Microscopy (SICM) was performed on a sample of ionogel. SICM involves a glass nanopipette filled with electrolyte, in ionogel experiments the same ionic liquid that was used in the ionogel synthesis was used (BMIM TFSI with 500 mM Li TFSI) and a glass slide with deposited ionogel immersed in a Petri dish containing the same ionic liquid electrolyte. In the experiments outlined below, a "hopping" mode of SICM was employed, which allowed for the recording of topography images, and scan response of the pipette at multiple locations on the surface. There are two states in which the SICM takes measurements, the first is the retracted state in which the pipette is far enough away from surface that measurements are not affected by the presence of the sample. The second state is the extended state where the pipette is close enough to the sample for its measurements to depend on the charges present on the sample. These measurements are taken with a Ag/AgCl electrode inside the pipette, and another inside the bulk electrolyte in the petri dish. This set up can be seen in figure 3.8.

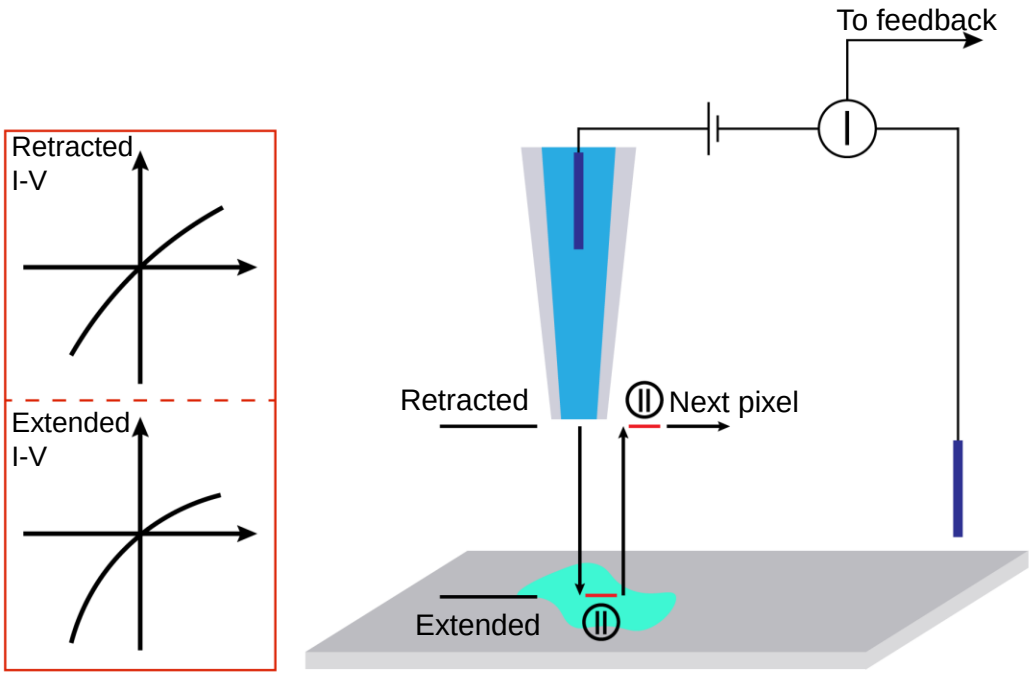

Figure 3.7: Schematic of the instrumental setup of SICM used to map the surface charges present on a sample.

At the beginning of each measurement the pipette starts in the retracted state and an I-V curve is taken. After the measurement is complete, the pipette approaches the sample and in the extended state another IV curve is recorded. The applied potential difference for each of these I-V curves was swept in a preset range, typically, -1.6 V to 1.6 V in 19 even steps. Examples of these I-V curves on glass and ionogel can be seen in figure 3.9.

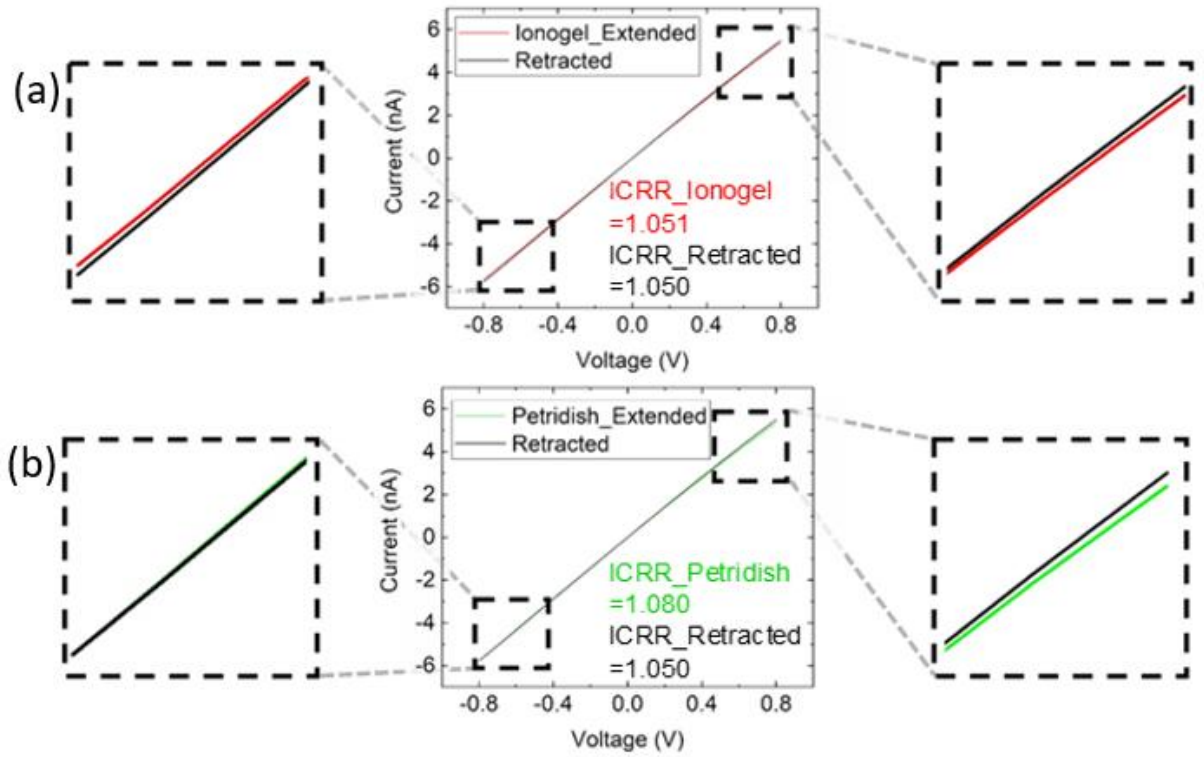

Figure 3.8: Extended I-V curves of (a) ionogel surface and (b) Petri dish surface are plotted together with the retracted I-V curve separately.

These I-V curves are used to calculate the ion current rectification ratios (ICRR)[1], which are defined by the following equation:

$$ICRR = \left|\frac{I_{-1.6\,V}}{I_{1.6\,V}}\right| \qquad 3.3$$

Where $I_{-1.6\,V}$ is the current value at -1.6 V and $I_{1.6V}$ is the current value at +1.6 V. The difference between ICRR while the probe is extended and ICRR while the probe is retracted was calculated and this value is directly related to the surface charge of the sample.

$$ICRR_{difference} = ICRR_{extended} - ICRR_{retracted} \quad 3.4$$

where $ICRR_{extended}$ and $ICRR_{retracted}$ represent rectification of the pipette in an extended and retracted position, respectively and $ICRR_{difference}$ is simply the difference between the two. The ICRR's are calculated at each topography point to create a correlating map of surface charges. Figure 3.10 shows examples of recorded data showing the topography image, $ICRR_{extended}$ and $ICRR_{retracted}$ as well as $ICRR_{difference}$ of the ionogel sample in ionic liquid. Experiments were performed in the area with a visible interface between a bare glass slide, and a portion with deposited ionogel. In order to gain an idea of how the surface charges compare to that of glass.

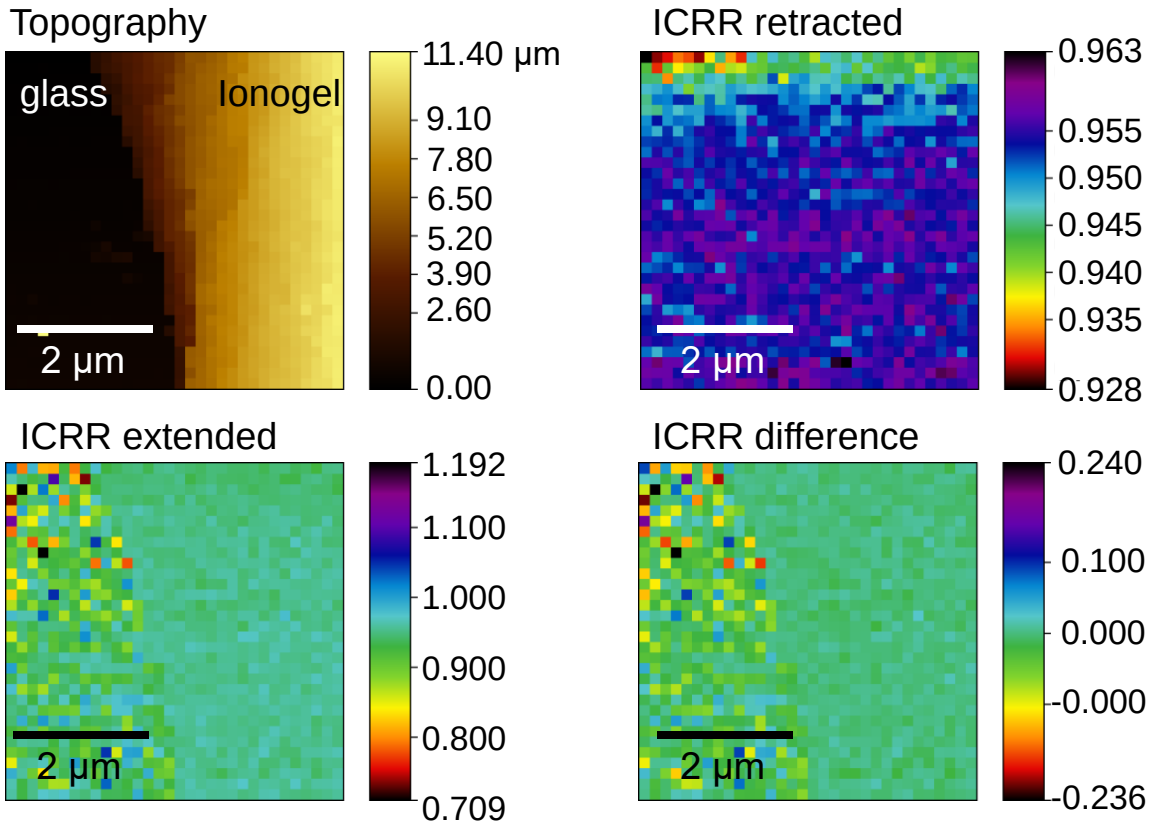

Figure 3.9: Topography and surface charge mapping of Ionogel from SICM on a petri dish

Even though all current-voltage curves recorded were nearly linear for the ionogel, there is a small degree of rectification observed when the pipette is above the glass surface, which would indicate the glass featured a small positive surface charge. The positive charge could stem from adsorption of Li^+ ions, reported before for negatively charged polymer films. I-V curves in the area with ionogel was characterized by significantly lower rectification degrees indicating the surface charges are screened by ionic liquid more efficiently in the ionogel than the glass slide.

3.3: TESTS IN $LiClO_4$ SOLUTIONS IN PROPYLENE CARBONATE

In order to provide additional evidence that the voids in the ionogel are interconnected and the ionogel fills the entire volume of the pores we have placed the pores in contact with a propylene carbonate solution of lithium perchloride. Propylene carbonate is miscible with the ionic liquid thus it was expected that the propylene carbonate would replace the ionic liquid in the ionogel network. A successful replacement of the electrolyte would be evidenced by the dependence of the measured conductance on the background electrolyte concentration. Figure 3.7 shows the IV curves taken from these measurements.

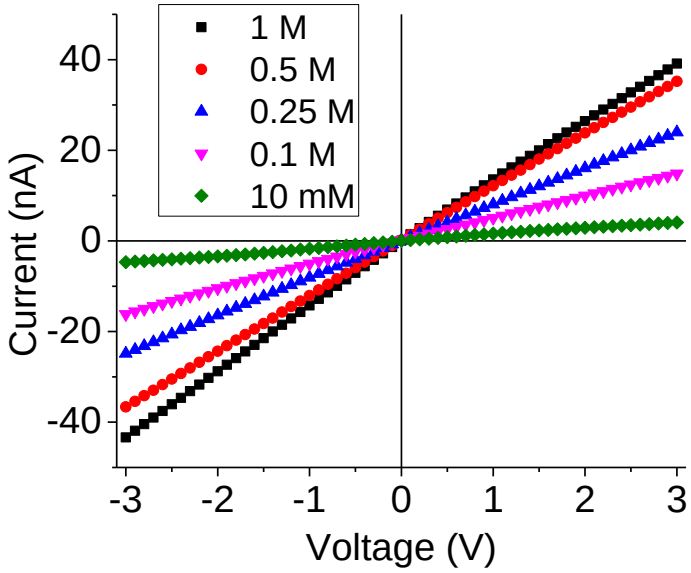

Figure 3.10: Example of current-voltage curves through a single 730 nm cylindrical pore with changing concentration of LiClO4 in propylene carbonate varying between 10 mM to 1 M

Figure 3.8 shows a magnitude of the conductivity calculated based on the pore geometry and resistance obtained from I-V curves. An increase of conductivity with the increase of $LiClO_4$ concentration in the bulk suggested that indeed ionic concentration in the ionogel is influenced by the bulk electrolyte. The magnitude of conductivity saturated at ~500 mM $LiClO_4$ and reached the magnitude observed with the ionic liquid. Note however that the ionic transport of $LiClO_4$ in PC is hindered in the ionogel compared to bulk measurements as well as recordings with an as-prepared pore, before ionogel deposition. We believe the lower ionic conductivity of the liquid electrolyte stems from its interactions with the silica surface reported before for the salt.

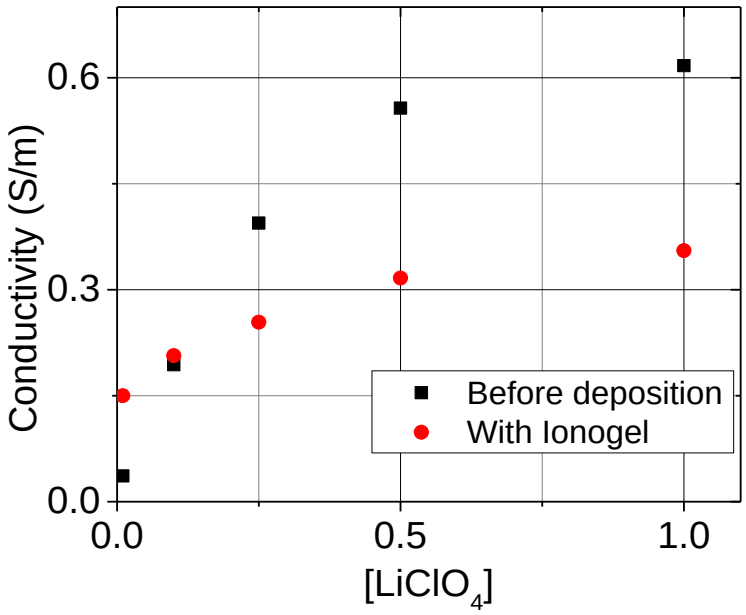

Figure 3.11: Conductivity of the pore before and after the ionogel was deposited as a function of the changing concentration of LiClO4 in the bulk liquid electrolyte.

Conclusions

The thesis laid the groundwork for probing ionic conductivity of solid electrolytes at the meso- and nanoscales. We provided two approaches to probe ion current carried by solid electrolytes. The future work will focus on probing solid electrolytes embedded in truly nanoscopic structures with diameters as small as few nanometers. We plan to do it with nanopores in silicon nitride films of tunable thickness.

REFERENCES

[1] R. B. Schoch, J. Han, and P. Renaud, "Transport phenomena in nanofluidics," *Rev. Mod. Phys.*, vol. 80, no. 3, pp. 839–883, 2008.

[2] I. Vlassiouk, S. Smirnov, and Z. Siwyt, "Ionic selectivity of single nanochannels," *Nano Lett.*, vol. 8, no. 7, pp. 1978–1985, 2008.

[3] C. Wei, A. J. Bard, and S. W. Feldberg, "Current Rectification at Quartz Nanopipet Electrodes," *Anal. Chem.*, vol. 69, no. 22, pp. 4627–4633, 1997.

[4] Z. Siwy and A. Fuliński, "Fabrication of a Synthetic Nanopore Ion Pump," *Phys. Rev. Lett.*, vol. 89, no. 19, pp. 4–7, 2002.

[5] H. S. White and A. Bund, "Ion current rectification at nanopores in glass membranes," *Langmuir*, vol. 24, no. 5, pp. 2212–2218, 2008.

[6] J. Cervera, B. Schiedt, and P. Ramírez, "A poisson/nernst-planck model for ionic transport through synthetic conical nanopores," *Europhys. Lett.*, vol. 71, no. 1, pp. 35–41, 2005.

[7] M. Ali, P. Ramirez, S. Mafé, R. Neumann, and W. Ensinger, "A pH-Tunable nanofluidic diode with a broad range of rectifying properties," *ACS Nano*, vol. 3, no. 3, pp. 603–608, 2009.

[8] Z. Siwy, L. Trofin, P. Kohli, L. A. Baker, C. Trautmann, and C. R. Martin, "Protein biosensors 'based on biofunctionalized conical gold nanotubes," *J. Am. Chem. Soc.*, vol. 127, no. 14, pp. 5000–5001, 2005.

[9] S. Howorka and Z. Siwy, "Nanopore analytics: sensing of single molecules," *Chem. Soc.*

Rev., vol. 38, no. 8, p. 2360, 2009.

[10] Y. Tian, L. Wen, X. Hou, G. Hou, and L. Jiang, "Bioinspired ion-transport properties of solid-state single nanochannels and their applications in sensing," *ChemPhysChem*, vol. 13, no. 10, pp. 2455–2470, 2012.

[11] W. Shi, A. K. Friedman, and L. A. Baker, "Nanopore Sensing," *Anal. Chem.*, vol. 89, no. 1, pp. 157–188, 2017.

[12] H. B. Park, J. Kamcev, L. M. Robeson, M. Elimelech, and B. D. Freeman, "Maximizing the right stuff: The trade-off between membrane permeability and selectivity," *Science (80-.).*, vol. 356, no. 6343, pp. 1138–1148, 2017.

[13] L. Xia, L. Yu, D. Hu, and G. Z. Chen, "Electrolytes for electrochemical energy storage," *Mater. Chem. Front.*, vol. 1, no. 4, pp. 584–618, 2017.

[14] A. M. Stephan, "Review on gel polymer electrolytes for lithium batteries," *Eur. Polym. J.*, vol. 42, no. 1, pp. 21–42, 2006.

[15] W. Li, Y. Pang, J. Liu, G. Liu, Y. Wang, and Y. Xia, "A PEO-based gel polymer electrolyte for lithium ion batteries," *RSC Adv.*, vol. 7, no. 38, pp. 23494–23501, 2017.

[16] M. Le Thai, G. T. Chandran, R. K. Dutta, X. Li, and R. M. Penner, "100k Cycles and Beyond: Extraordinary Cycle Stability for MnO2Nanowires Imparted by a Gel Electrolyte," *ACS Energy Lett.*, vol. 1, no. 1, pp. 57–63, 2016.

[17] K. Kerman, A. Luntz, V. Viswanathan, Y.-M. Chiang, and Z. Chen, "Review—Practical Challenges Hindering the Development of Solid State Li Ion Batteries," *J. Electrochem. Soc.*, vol. 164, no. 7, pp. A1731–A1744, 2017.

[18] T. S. Plett, W. Cai, M. Le Thai, I. V. Vlassiouk, R. M. Penner, and Z. S. Siwy, "Solid-State Ionic Diodes Demonstrated in Conical Nanopores," *J. Phys. Chem. C*, vol. 121, no. 11,

pp. 6170–6176, 2017.

[19] T. S. Plett, M. Le Thai, J. Cai, I. Vlassiokiv, R. Penner, and Z. Siwy, "Ion Transport in Gel and Gel-Liquid Systems for LiClO4-doped PMMA at the Meso- and Nanoscales," *Nanoscale*, pp. 16232–16243, 2017.

[20] D. S. Ashby, R. H. DeBlock, C. H. Lai, C. S. Choi, and B. S. Dunn, "Patternable, Solution-Processed Ionogels for Thin-Film Lithium-Ion Electrolytes," *Joule*, vol. 1, no. 2, pp. 344–358, 2017.

[21] P. Nelson, "Biological Physics: Energy, Information, Life," *W.H. Free. Company, New York, NY*, 2004.

[22] R.F. Probstein, "Physicochemical Hydrodynamics: An Introduction, 2nd Edition," *John Wiley Sons, Inc., New York, NY*, 1994.

[23] A. A. Kornyshev, "Double-layer in ionic liquids: Paradigm change?," *J. Phys. Chem. B*, vol. 111, no. 20, pp. 5545–5557, 2007.

[24] M. V. Fedorov and A. A. Kornyshev, "Ionic liquid near a charged wall: Structure and capacitance of electrical double layer (J. Phys.Chem.B (2009) 112B (113) 10.1021/jp900599h)," *J. Phys. Chem. B*, vol. 113, no. 13, p. 4500, 2009.

[25] R. Spohr, "Method and device to generate a predetermined number of ion tracks," DE 2951376, 1983.

[26] Z. Zhu, Y. Maekawa, Q. Liu, and M. Yoshida, "Influence of UV light illumination on latent track structure in PET," *Nucl. Instruments Methods Phys. Res. Sect. B Beam Interact. with Mater. Atoms*, vol. 236, no. 1–4, pp. 61–67, 2005.

[27] W. DeSorbo, "Ultraviolet effects and aging effects on etching characteristics of fission tracks in polycarbonate film," *Nucl. Tracks*, vol. 3, no. 1–2, pp. 13–32, 1979.

[28] C. Chad Harrell, Z. S. Siwy, and C. R. Martin, “Conical nanopore membranes: Controlling the nanopore shape,” *Small*, vol. 2, no. 2, pp. 194–198, 2006.

[29] B. T.L., H. E. LeMay Jr., and B. E. Bursten, “Chemistry: The Central Science, 8th Edition,” *Prentice Hall, Up. Saddle River, NJ*, 2000.

[30] P. Y. Apel, Y. E. Korchev, Z. Siwy, R. Spohr, and M. Yoshida, “Diode-like single-ion track membrane prepared by electro-stopping,” *Nucl. Instruments Methods Phys. Res. Sect. B Beam Interact. with Mater. Atoms*, vol. 184, no. 3, pp. 337–346, 2001.

[31] D. Membreno, L. Smith, and B. Dunn, “Silica sol-gel chemistry: Creating materials and architectures for energy generation and storage,” *J. Sol-Gel Sci. Technol.*, vol. 70, no. 2, pp. 203–215, 2014.

[32] A. Guyomard-Lack, P.-E. Delannoy, N. Dupré, C. V. Cerclier, B. Humbert, and J. Le Bideau, “Destructuring ionic liquids in ionogels: enhanced fragility for solid devices,” *Phys. Chem. Chem. Phys.*, vol. 16, no. 43, pp. 23639–23645, 2014.